Stress-based Model for Lifetime Estimation of Bond-Wire Contacts using Power Cycling Tests and Finite Element Modelling

Nausicaa Dornic, Zoubir Khatir, Son-Ha Tran, Ali Ibrahim, Richard Lallemand, Jean Pierre Ousten, Jeff Ewanchuk, Stefan Mollov

This article has been accepted for publication in a future issue of this journal, but has not been fully edited. Content may change prior to final publication. Citation information: DOI 10.1109/JESTPE.2019.2918941, IEEE Journal of Emerging and Selected Topics in Power Electronics

Stress-based Model for Lifetime Estimation of Bond-Wire Contacts using Power Cycling Tests and Finite Element Modelling

N. Dornic, Z. Khatir, S-H. Tran, A. Ibrahim, R. Lallemand, J.P. Ousten, J. Ewanchuk, S. Mollov

***Abstract*— In this paper, a lifetime model for bond wire contacts of Insulated Gate Bipolar Transistors (IGBT) power modules is reported. This model is based on power cycling tests obtained under accelerated conditions and a finite element model taking into account the electrical, thermal and mechanical coupling. It allows to estimate the bond-wires lifetime for a large scale of junction temperature swing amplitudes (ΔT_j) and stress durations (t_{on}). To build it, a numerical design of experiment was performed in both high and low stress values (ΔT_j). Then, a strain-life curve has been constructed where average strain values on a defined volume around the contact areas between top-metallization and the most exposed bond-wires to fatigue and lift-off have been used. As result, it has been shown that the total strain is linearly dependent with ΔT_j and power law dependent with t_{on}. The combination of the strain-life relation and the strain dependency with stress parameters leads to the lifetime relationship. The obtained lifetime model has been satisfactorily validated with some additional experimental points obtained from literature and with a large range of values for t_{on}. This methodology can easily be replicated to other structures and is quite generic.**

***Index Terms*— Power cycling, lifetime model, finite element modeling, stresses, strains, IGBT, power module, wire-bonds, accelerated ageing, junction temperature.**

I. Introduction

POWER semiconductor devices are the key components of power electronic systems. They are also the weak point of these systems in terms of reliability. During operations, they undergo high stresses (ambient temperature, temperature cycling, humidity, etc…). As commonly known, due to temperature cycling and differences in the coefficient of thermal expansion of materials, these devices are subjected to thermo-mechanical damage accumulation, which affects their lifetime and therefore impacts the reliability of the power modules [1-4].

Manufacturers are faced with the need to provide devices that are not only reliable but also compatible with a predictable maintenance schedule. Indeed, from an economic point of view, it is less detrimental to perform a planned maintenance with the replacement of these systems than to undergo a sudden stop due to a failure. It is therefore necessary to develop diagnostic tools in order to predict the remaining lifetime of equipment for maintenance purpose before any failure occurrence. To this end, numerous lifetime models of power electronic devices have been developed. They can be divided in three categories: empirical models [6-8], physics-based models [9-18] and data-driven or stochastic models [19-24].

Empirical lifetime models have been built from numerous accelerated power cycling tests. However, these models based on low cycle fatigue results do not have predictive capabilities outside the explored test conditions and an extrapolation must be done when applying the models from accelerated tests to field conditions, i.e. under high cycle fatigue conditions.

Physics-based lifetime models are driven by physics-of-failure (PoF) analyses and can provide a promising alternative to empirical models [5]. These models can be split in two main categories: stress-based models [9-12] and degradation-based models [13-18]. Both types can be used for remaining lifetime prediction and extrapolation from accelerated to the field operating conditions. In the first type, lifetime is related to the stress experienced, e.g. junction temperature swings (ΔT_j) and stress durations (t_{on}), through mechanical or physical quantities such as strains and energy densities. In the latter, the lifetime is related to the stress undergone through material degradation, cracking, crack propagation, recrystallization.

The aim of this paper is to propose a stress-based lifetime modeling approach applied to top-side interconnection (wire-bond contact) of an IGBT power module. The approach consists in carrying out accelerated aging tests in order to obtain the corresponding number of failure cycles. At the same time, simulations are performed in order to reproduce experimental loads and stresses as accurately as possible using electrical-thermal and mechanical coupled finite element models. From simulation results, inelastic and elastic strains will be extracted in same accelerated conditions as in experience and will be related to the lifetime (N_f) obtained experimentally. The main assumption is to say that the obtained relationship between

This manuscript has been submitted on January 13, 2019.

N. Dornic, S.H. Tran, Z. Khatir, A. Ibrahim, R. Lallemand, and J.P. Ousten are with the SATIE laboratory, IFSTTAR, 25 allee des marronniers, 78000 Versailles, France, (nausicaa.dornic@ifsttar.fr, zoubir.khatir@ifsttar.fr, son-ha.tran@ifsttar.fr, ali.ibrahim@ifsttar.fr, richard.lallemand@ifsttar.fr, jean-pierre.ousten@ifsttar.fr).

J. Ewanchuk and S. Mollov are with Mitsubishi Electric R&D Centre Europe (MERCE), 1, allee de Beaulieu CS 10806, 35708 Rennes, France, (J.Ewanchuk@fr.merce.mee.com, S.Mollov@fr.merce.mee.com).

This article has been accepted for publication in a future issue of this journal, but has not been fully edited. Content may change prior to final publication. Citation information: DOI 10.1109/JESTPE.2019.2918941, IEEE Journal of Emerging and Selected Topics in Power Electronics

strains and lifetime can be extended to low stress (ΔT_j), in non-accelerated conditions. This hypothesis can be made because the modules used were chosen to present only one mode of degradation, i.e. the bond-wire lift-off. In this paper, the temperature swing amplitude (ΔT_j) and the time duration (t_{on}) of the applied stress, i.e. the heating time, have been considered for the lifetime model. Nevertheless, the t_{on} effect has been assessed thanks to experimental results. Taking into account this parameter in the finite element model requires the consideration of specific time-dependent behavioral laws, such as creep, for top-side metallization and wire-bond materials. This will be the subject of a future paper.

II. POWER CYCLING TESTS METHODOLOGY AND RESULTS

A. Test circuit and protocol

In order to build the lifetime model, accelerated aging tests have been performed on IGBT power modules. These latter are commercially available SKIM63 (1200V-300A) from Semikron. These devices are six-pack modules with three individual phase legs on separated DBC substrates. These power modules were chosen for their robust die attach in order to concentrate the degradations only in the topside interconnections. The chips are all sintered with a nanoparticle silver paste, making the connections stronger than with classical solders. Hence, the degradations observed concern only the metallization and the bonds contacts. The power modules are mounted in a water-cooler heat-sink device with a thermal grease interface. In order to reach high temperature swing levels, a 5-mm-thick aluminum plate is inserted between the module and the cooling device with a second thermal grease layer.

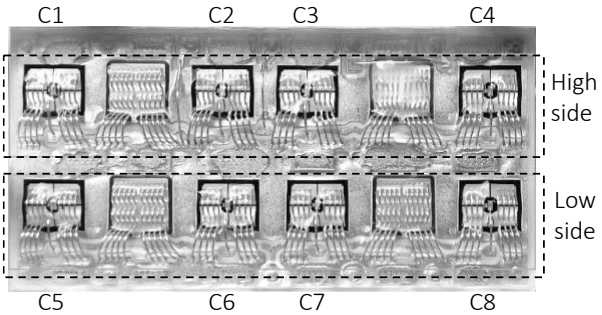

Fig. 1: Substrate of SKIM63 power module from Semikron.

As shown in the circuit schematic in fig.2, the power cycles are performed on 3 modules at a time for which only the central leg is tested (see fig.1). This constitutes 2 DUTs respectively high side and low side switches per power module.

The aging consists on repetitive cycles of self-heating and cooling phases. As test parameters, the minimum junction temperature (T_{jmin}) was set to 35°C, two stress durations (t_{on}) have been tested: 3s and 20s. The cooling duration (t_{off}) is twice as long as the heating duration (t_{on}) in order to reach the reference temperature of the cooling system at the end of each cycle, i.e. 6s and 40s respectively. The power devices undergo thermal stresses due to temperature swings ΔT_j between a maximum (T_{jmax}) and a minimum junction temperature (T_{jmin}) depending on the setting parameters. The DC current load (I_L) is set in order to reach the targeted temperature swings (110°C, 90°C and 70°C), see table I.

All electrical and thermal measurements are monitored and recorded with a data acquisition system (Dewetron). The switching sequence is controlled by auxiliary power MOSFETs (fig.2). A permanent low current (I_{sense}=50mA) is flowing through the devices under test (DUTs) in order to get the junction temperature (T_j) by a thermo-sensitive electrical parameter (TSEP), i.e the collector-emitter voltage ($V_{CE}@V_{GE}$=15V). The case temperature, below each IGBT chip of the central leg, and inlet water temperature are measured by close thermocouples for evaluating junction-to-case (R_{thjc}) and junction-to-water (R_{thjw}) thermal resistances.

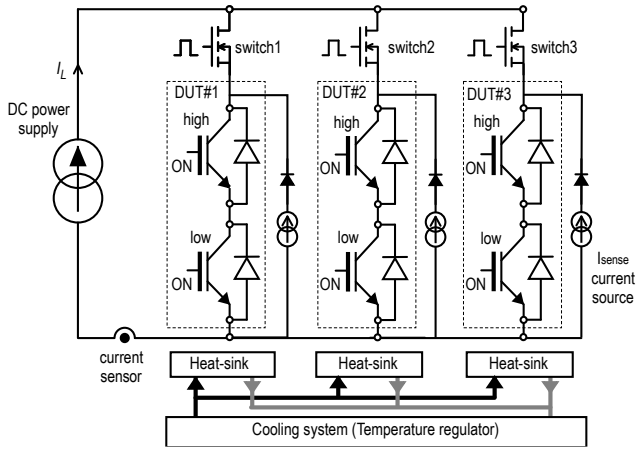

Fig. 2: Schematic power cycling test circuit.

The chosen ageing indicators are collector-emitter voltage drop (V_{CE}) and junction-to-water thermal resistance (R_{thjw}). These parameters are always measured in the same conditions before, during and after the aging in a static characterization phase. During the power cycling, the aging is automatically and regularly interrupted and the characterizations of ageing indicators are performed.

The measured voltage V_{CE} may possibly include a thermal contribution due to any increase in thermal resistance from possible delamination of the die attach. So, this latter possible contribution needs to be removed from the measured V_{CE} in order to detect only the contribution due to top-die interconnection degradations. Thus, a correction on the measured V_{CE} is done to get only the degradations related to top-metal and bonding wires contacts. This correction consists in subtracting the part of V_{CE} which can possibly be due to an increase of temperature related to an increase of thermal resistance, if any solder delamination occurs.

For that purpose, a thermal calibration is carried out at the beginning of aging tests, before any degradation. During this calibration, the drop voltage V_{CE} is recorded and plotted in a temperature range from 75°C to 90°C after reaching thermal equilibrium. This variation in temperature is obtained by modifying the inlet water flow to change the cooling performance. The obtained dependence between the junction temperature (T_j) and the drop voltage (V_{CE}) is linear and offers an average corrective coefficient of V_{CE} with temperature. This enables a correction in V_{CE} to account for the possible difference

This article has been accepted for publication in a future issue of this journal, but has not been fully edited. Content may change prior to final publication. Citation information: DOI 10.1109/JESTPE.2019.2918941, IEEE Journal of Emerging and Selected Topics in Power Electronics

between the measured junction temperatures at initial and actual characterizations. As expected, all tests have led to insignificant R_{th} increase.

B. Test results

As results, all tested devices have failed by bond-wire lift-off. As an illustration, it can be seen in fig.3 the evolution during aging of the relative variation of V_{CE} for the 3 modules tested at ΔT_j = 90°C. No variation in thermal resistance was detected, indicating that no delamination has occurred in the structure. This result is confirmed by scanning acoustic microscopy (SAM) analyses performed after the ageing for both long (Fig.4a) and short cycling (Fig.4b). Hence, the degradation of wire bonds is the only failure mode.

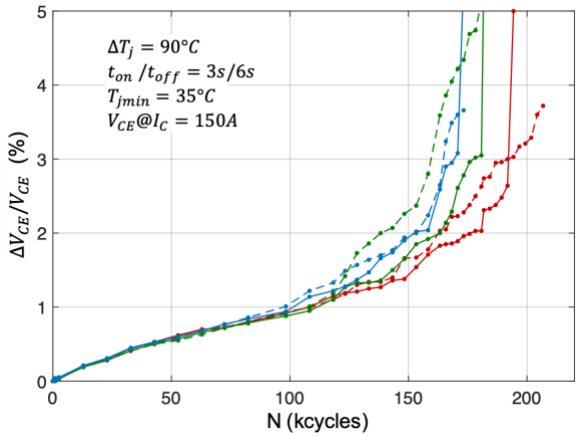

Fig. 3: Example of evolution of relative variation in V_{CE} during aging test.

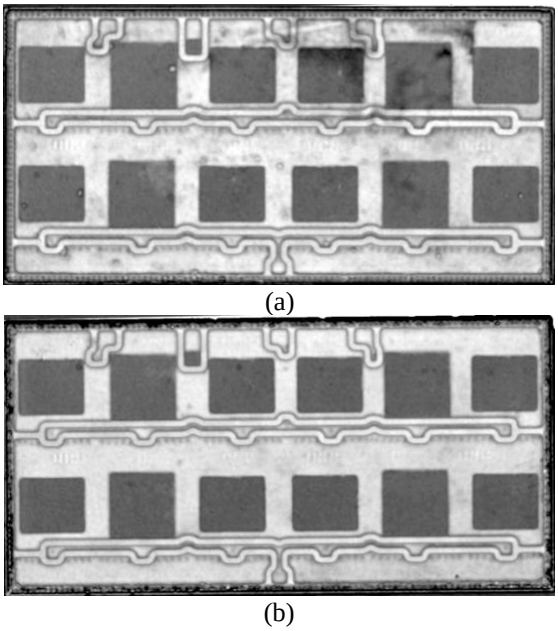

(a)

(b)

Fig. 4. SAM image of a SKIM63 module under long cycling (a) - Test conditions: T_{jmin} = 35°C, ΔT_j = 110°C, t_{on}/t_{off} = 20s/40s, and under short cycling (b) - Test conditions: T_{jmin} = 55°C, ΔT_j= 90°C, t_{on}/t_{off} = 3s/6s.

The full test conditions and results in number of cycles to failure (N_f) are given in table I for t_{on} = 3 s and in table II for t_{on}= 20 s. In these tables, the load DC current, the N_f value for each tested devices and the averaged N_f value for each test condition are given. As expected, lifetime is reduced when t_{on} is increased.

TABLE I
TEST CONDITIONS AND POWER CYCLING RESULTS (t_{on}=3S)

ΔT_j(°C)	T_{jmin}(°C)	I_L (A)	N_f (kcycles)	N_f mean value (kcycles)
110	35	260	[74, 66, 78]	73
90	35	240	[207, 182,173]	187
70	35	210	[934, 739, 904]	860

TABLE II
TEST CONDITIONS AND POWER CYCLING RESULTS (t_{on} =20S)

ΔT_j(°C)	T_{jmin}(°C)	I_L (A)	N_f (kcycles)	N_f mean value (kcycles)
110	35	230	[35, 40, 35]	37
90	35	205	[96, 97, 95]	96
70	35	185	[485, 482, -]	483

III. FINITE ELEMENT MODEL AND RESULTS

Finite element modelling is required in order to compute stress and strain development within the power module assembly during power cycling. However, obtaining correct stress and strain maps inside the structure requires : i) detailed knowledge of the geometry as well as material properties and behavior laws and ii) the thermal stresses the more accurately as possible, i.e. the correct maps of temperatures and temperature gradients. For this purpose, the electro-thermo-mechanical coupling problem must be taken into account. In particular, a special attention must be kept for the top-metal layer in the active areas of the dies and the bond-wires.

A. Description of the finite element model geometry

We recall that only the central leg has been tested and only bond-wire lift-off of IGBT chips occurred in experimental tests. So, as expected, the results of interest are at the level of metallization and contacts with the bonding wires of the corresponding substrate. The lateral substrates therefore have no thermomechanical influence and can be avoided in the numerical model for simplification reasons.

The model is shown in figs.5 and 6. The power module is made-up of the central substrate which is mounted on an aluminum heat-sink. An aluminum plate is inserted between the heat-sink and the power module as for experimental tests to reach high temperature variations. Two thermal interface materials (TIM) layers are used as shown in fig.5 to ensure the thermal contact between the substrate and aluminum plate and between the aluminum plate and the heat-sink.

The geometrical model of the substrate is shown in fig.6. All the IGBT dies are taken into account with their thin top-metal layers. The four diodes are not considered in the model. The metallization layers cover the active areas of the dies. A direct copper bond (DCB), with an aluminum nitride (AlN) ceramic, is used as substrate where the eight chips are attached on copper patterns (copper1 and copper2).

This article has been accepted for publication in a future issue of this journal, but has not been fully edited. Content may change prior to final publication. Citation information: DOI 10.1109/JESTPE.2019.2918941, IEEE Journal of Emerging and Selected Topics in Power Electronics

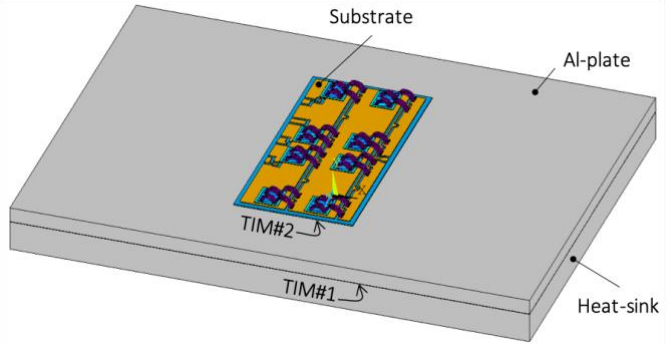

Fig. 5: The whole geometrical model, only the central leg is stressed.

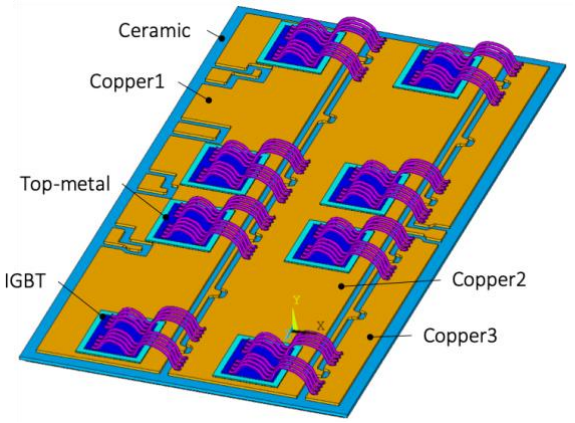

Fig. 6: Details of the geometrical model of the central substrate.

B. Material nature and properties

All materials, with their dimensions, are given in table III. These are ranked from top to bottom, from the wire-bonds to the heat-sink. The material properties of the power assembly, used for the finite elements model, are given in table IV. Fragile materials, like silicon and ceramic, exhibit deformation limited to elastic domain only, i.e. linear properties are used for them. In the temperature range of active cycling tests, aluminum is modeled by elastoplastic behavior laws as visible in fig.7. The Ag sintering layers are generally considered as viscoplastic materials. Nevertheless, they have been considered here as elastic. This simplifying assumption is justified by the high rigidity of the silicon chips preventing the lower material layers, including the die-attach, from having an impact on the deformations of the metallization and the wires in the top-side. The mechanical behavior of the die-attaches therefore has no impact on the mechanical quantities on the top-side of the chips. Their consideration is only justified for solving the electrothermal problem and not the mechanical problem.

Concerning the electrical behavior of IGBTs, since the power cycling is in DC mode, only Joule effects is considered. Moreover, it is only necessary to have representative power losses within the dies. Thus, these ones are considered as conductive layers with anisotropic resistivities. Since IGBT chips can be considered as multiple elementary IGBT cells in parallel, the current flows only in the vertical axis (i.e. through the thickness of the dies). So, in order to simulate such "vertical" conduction, the in-plane resistivities data input for IGBTs are supposed high enough $\rho_{x-igbt} = \rho_{y-igbt} = 10^6\ \Omega m$, whereas the vertical resistivity is fitted in order to have the same on-state voltage as in experiments. This is to have the same dissipated power in the heating phase than in experiments. Static I-V characteristics are plotted for different temperatures with a curve tracer, so that the temperature effect on the V_{CE} is also taken into account :

$$V_{CE}(T_j) = k_1(T_j)\, I_c^{k_2(T_j)} + k_3(T_j) \quad (1)$$

with,

$$\begin{cases} k_1(T_j) = 4.75 \times 10^{-5}\ T_j + 0.01394 \\ k_2(T_j) = 1.99 \times 10^{-4}\ T_j + 0.7453 \\ k_3(T_j) = -1.57 \times 10^{-3}\ T_j + 0.8069 \end{cases} \quad (2)$$

In these relations, T_j is in °C and V_{CE} in Volts.

TABLE III
DIMENSIONS AND NATURE OF MATERIALS

Parameter	Material	Thickness (µm)	Dimensions (mm x mm)
Bondwires	Aluminum	∅ 380µm	-
Top-metal (IGBT)	Aluminum	10	6.2 x 7.6
IGBTs	Silicon	140	7.7 x 9.1
Ag-Sinter	Silver	20	see IGBT
Ceramic	AlN	380	39 x 78
Pattern	Copper	300	36 x 75
TIM1	Thermal grease	100	38 x 77
Plate	Aluminum	5000	170 x 124
TIM2	Thermal grease	100	170 x 124
Heat-sink	Aluminum	10000	170 x 124

TABLE IV
MATERIAL PROPERTIES

	Al	Si	Cu	AlN	Ag	TIM
Density	2700	2330	8960	3780	7350	-
CTE (ppm/K)	23.5	4.1	17	8	19.6	-
Young mod. (GPa)	76	131	97	370	6.28	-
Poisson coef.	0.33	0.3	0.34	0.2	0.37	-
Non-linear properties	Fig.7	-	Fig.7	-	-	-
Thermal cond. ($W.m^{-1}.K^{-1}$)	238	124	390	24	250	2
Specif. Heat ($J.Kg^{-1}K^{-1}$)	897	750	390	830	230	-
Electrical Resistivity (Ω.m)	27.10^{-9}	comment	17.10^{-9}	1.10^{12}	4.10^{-8}	1.10^{20}

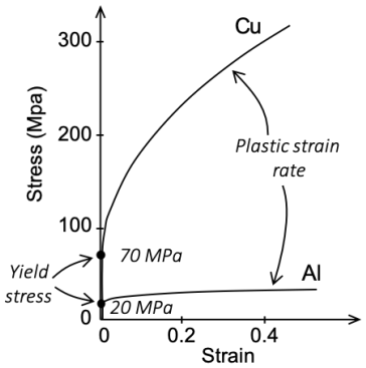

Fig. 7: Elasto-plastic stress-strain behaviors for aluminum and copper.

This article has been accepted for publication in a future issue of this journal, but has not been fully edited. Content may change prior to final publication. Citation information: DOI 10.1109/JESTPE.2019.2918941, IEEE Journal of Emerging and Selected Topics in Power Electronics

C. Boundary conditions

As electrical boundary conditions, the reference for voltage (V=0) is applied to copper3 pattern and the load current (I_L) is injected into copper1 pattern (see fig.6).

As thermal boundary conditions, a convective condition is assumed at the bottom face of the heat-sink, with a convective coefficient of h = 4000 W/m^2.K and a bulk temperature of 35°C. All other boundaries are considered as adiabatic.

As mechanical boundary conditions, three among the four corners of the heat-sink are fixed with no displacement allowed.

D. Simulation Results

Table VI gives the numerical experimental design carried-out in DC mode. The simulated values in ΔT_j are: 15, 25, 55, 70, 90 and 110°C. For an effective comparison with the tests, the ΔTj values here are the junction temperature mean values calculated over the IGBT chip active area that can be compared with the TSEP measurements.

Concerning loads, a succession of 5 cycles of power current is simulated as schematically shown in fig.8. The heating durations (t_{on}) are set to 3s and the cooling durations (t_{off}) to 10s to allow the temperature to reach T_{jmin}. Load currents (I_L) are then determined to reach the desired ΔT_j values. In table VI, simulated load currents are given for comparison to experimental ones (see tables I and II). It can be seen that for ΔT_j = 110°C, 90°C and 70°C, currents used as input in the model are almost the same as the experimental DC ones, the small difference being probably the result of an inexact definition in the geometry or the material properties used in the model.

TABLE VI
NUMERICAL EXPERIMENTAL DESIGN (t_{on}=3S)

ΔT_j(°C)	110	90	70	55	25	15
I_L (A)	272	256	225	189	122	80

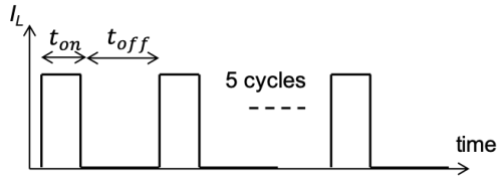

Fig. 8: Schematic load current cycles for numerical simulations.

It is necessary to simulate a few cycles for the mechanical results, e.g. strain variation per cycle, to reach stabilized values from one cycle to another. As illustration, fig.9 gives the temperature distribution over the substrate at the end of a power cycle for the first simulated case (I_L = 272 A and t_{on} = 3s). The average temperature over the IGBT active area is 145°C. This is consistent with a minimum junction temperature of 35°C and a T_j temperature swing of 110°C.

As outputs, some physical quantities averaged over a defined volume have been computed. Among them, a focus is made on the elastic and inelastic strain variations per cycle at the metallization layer of the IGBT chip near the bond contacts where lift-off occur experimentally. The concerned bond contacts are shown in fig.10 inside the white rectangle. This figure shows the plastic strain distribution at the end of a heating phase over the metallization layer of one of the four central IGBTs.

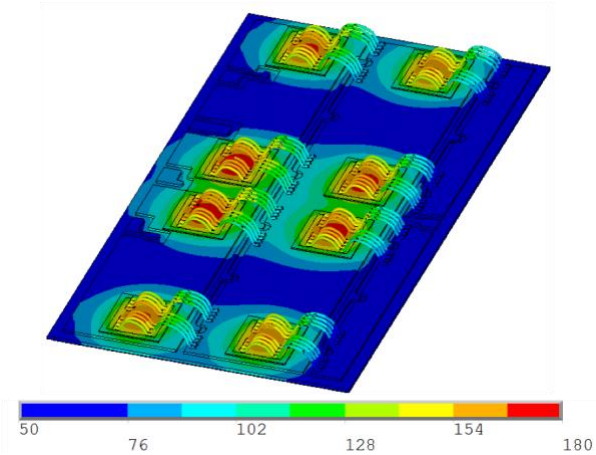

Fig. 9: Temperature map (in °C) within the substrate (I_L = 272 A, t_{on}=3s).

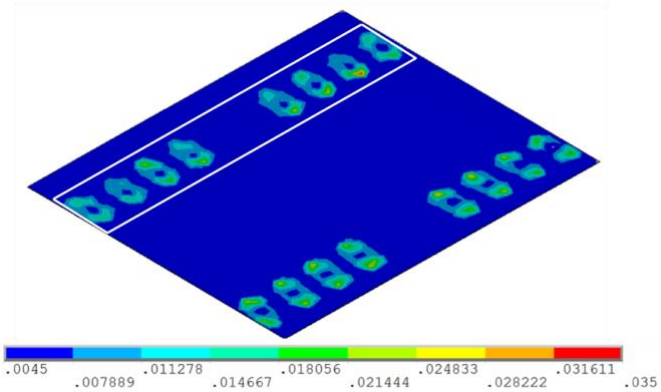

Fig.10: Plastic strain distribution at the end of a heating phase over the metallization layer of the high side IGBT (I_L = 272A, t_{on}=3s).

In order to avoid singular values of such quantities, averaged values of elastic and plastic strains over a defined volume of this metallization is considered:

$$\Delta x = \frac{\sum_i \Delta x_i \cdot v_i}{\sum_i v_i} \quad (3)$$

The considered volume is shown by the white rectangle in fig.10 and consists on a number of finite element volumes. In relation (3) Δx stands for the averaged value, i.e. elastic variation per cycle ($\Delta\varepsilon_{el}$) or plastic variation per cycle ($\Delta\varepsilon_{pl}$); Δx_i is the mean value of quantity Δx over the elementary volume i and v_i is the volume of the corresponding volume element. The summation is done over the volume elements contained in the defined volume.

As results, it can be seen in fig.11, the evolution during some cycles of junction temperature of the high side IGBT (average value over the active area), the plastic strain and elastic strain for I_L = 272 A and t_{on} = 3s conditions. Concerning strain variations, the von Mises representation has been chosen. During the power cycle, the top-metal material successively undergoes cyclic tensile and compressive forces so that it undergoes plastic deformations in compression then in traction. Almost the same amount of elastic strain occurs during the heating and cooling phases, the elastic strain variation during a

This article has been accepted for publication in a future issue of this journal, but has not been fully edited. Content may change prior to final publication. Citation information: DOI 10.1109/JESTPE.2019.2918941, IEEE Journal of Emerging and Selected Topics in Power Electronics

full cycle is the sum of the corresponding values during "on" and "off" phases.

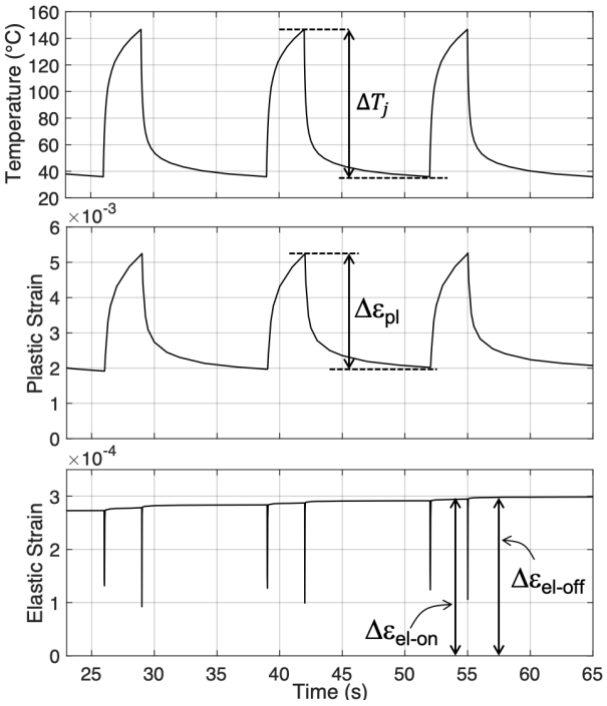

Fig.11: Evolution over some cycles of junction temperature (upper graph), plastic strain (central graph) and elastic strain (lower graph).

In table VII, it is given the values of $\Delta\varepsilon_{el}$ and $\Delta\varepsilon_{pl}$ respectively for ΔT_j =110, 90 and 70°C from simulation results for test condition t_{on} = 3s:

TABLE VII
ELASTIC AND PLASTIC VARIATION PER CYCLE (t_{on}=3s)

ΔT_j(°C)	$\Delta\varepsilon_{el}$	$\Delta\varepsilon_{pl}$
110	5.93×10^{-4}	3.17×10^{-3}
90	5.78×10^{-4}	2.46×10^{-3}
70	5.62×10^{-4}	1.81×10^{-3}

These calculated values in $\Delta\varepsilon_{el}$ and $\Delta\varepsilon_{pl}$ obtained for ΔT_j = 70, 90 and 110°C can be plotted in a graph $\Delta\varepsilon_{el} = f(N_f)$ and $\Delta\varepsilon_{pl} = g(N_f)$, where corresponding N_f are given in table I. Theoretically, it is expected linear curves in log-log axes [25]. This is visible in fig.12 with the segments of solid lines (blue for elastic strains and red for plastic strains).

So, from these three points in ΔT_j, the following relationships can be identified :

$$\Delta\varepsilon_{el} = A.N_f^{-a} \quad (4)$$

$$\Delta\varepsilon_{pl} = B.N_f^{-b} \quad (5)$$

with: $A = 7.48 \times 10^{-4}$; $a = 2.11 \times 10^{-2}$; $B = 3.66 \times 10^{-2}$; $b = 0.221$.

It must be kept in mind that this model does not take into account the duration of stress, the behavior laws used for aluminum (metallization and bond-wires) being time-independent. To this end, it would have been necessary to introduce creep laws for these materials. These data are extremely difficult to characterize and literatures does not provide them for the considered geometries (thin films and wires bond).

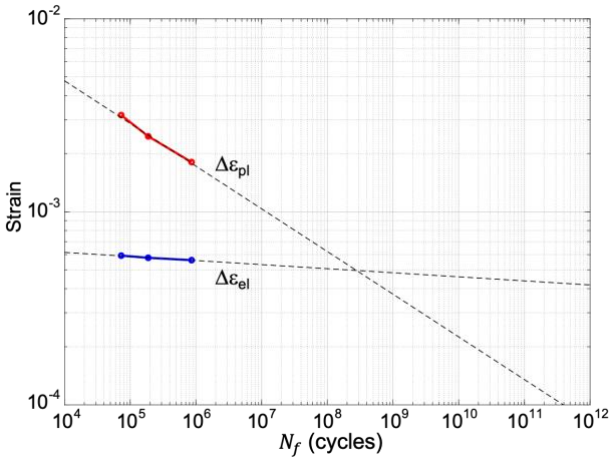

Fig.12: Elastic and plastic strains dependence with lifetime

Since the lifetime is assumed to be unequivocally related to the strain variations, the relationships between strain and N_f, i.e. eq.(4) and (5), remain valid whatever the t_{on}. Thus, the strain values obtained for t_{on}=3s can be considered as a relative reference and the results in N_f obtained for t_{on} = 20s allows to get the new corresponding strains (for t_{on} = 20s), see table VIII.

TABLE VIII
ELASTIC AND PLASTIC VARIATION PER CYCLE (t_{on}=20s)

ΔT_j(°C)	$\Delta\varepsilon_{el}$	$\Delta\varepsilon_{pl}$
110	5.99×10^{-4}	4.18×10^{-3}
90	5.87×10^{-4}	3.49×10^{-3}
70	5.68×10^{-4}	2.60×10^{-3}

Furthermore, in fig.13 are plotted the dependences in ΔT_j of elastic and plastic strains variations per cycle as well as total strain, where:

$$\Delta\varepsilon_{total} = \Delta\varepsilon_{el} + \Delta\varepsilon_{pl} = A.N_f^{-a} + B.N_f^{-b} \quad (6)$$

Elastic strain should be theoretically zero at ΔT_j = 0°C, then saturates almost to ΔT_j = 30°C around a value of 5×10^{-4}. Plastic strain begins to rise from ΔT_j = 15°C and then varies almost linearly with ΔT_j. We can note that plastic strain is equivalent to elastic strain at about ΔT_j = 30°C.

Since no strains are expected for ΔT_j = 0°C, we can write a linear relationship between total strain per cycle and ΔT_j :

$$\Delta\varepsilon_{total} \approx k\,\Delta T_j \quad (7)$$

For a given ΔT_j, it is expected that the inelastic strain $\Delta\varepsilon_{pl}$ should be t_{on} dependent. Indeed, longer stress durations, i.e. higher t_{on} values, lead to shorter lifetimes, resulting in larger deformations per cycle. Thus, the coefficient k depends on the value of the parameter t_{on}. Since for t_{on} = 0, the coefficient k

This article has been accepted for publication in a future issue of this journal, but has not been fully edited. Content may change prior to final publication. Citation information: DOI 10.1109/JESTPE.2019.2918941, IEEE Journal of Emerging and Selected Topics in Power Electronics

must itself be zero, the relationship between k and t_{on}, should be of the form :

$$k \approx \alpha\, t_{on}^{\beta} \tag{8}$$

From results given in tables VII and VIII, the value of k can be obtained for t_{on} = 3s and 20s : $k_{3s} \approx 3.6 \times 10^{-5} K^{-1}$ and $k_{20s} \approx 3.8 \times 10^{-5} K^{-1}$. From these values, α and β parameters can be identified: $\alpha = 3.18 \times 10^{-5}$; $\beta = 6.6 \times 10^{-2}$

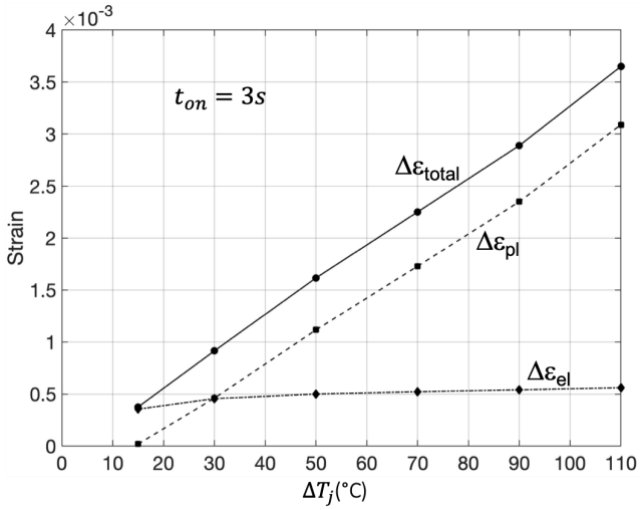

Fig.13: Dependence with junction temperature swing (ΔT_j) of the elastic, plastic and total strain variation per cycle for t_{on}=3s condition.

IV. Lifetime Estimation and Extrapolation for Low ΔT_j

The relations (4) and (5) can be plotted and extrapolated in fig.14 (red and blue dashed lines) as well as the total strain per cycle (6), i.e. the black dashed curve.

By using relation (7), it is possible to place in the black dashed curve any total strain with its corresponding ΔT_j and so to extrapolate for low ΔT_j values, see fig.14. In this figure, it can be noticed that for low N_f cycles, with high ΔT_j values, plastic strains are dominant leading to a Coffin-Manson's law behavior [25] whereas for high N_f values, corresponding to low ΔT_j values, elastic strains are dominant and Basquin's law fatigue takes place [26, 27].

By eliminating $\Delta\varepsilon_{total}$ between (6) and (7) we have a non-trivial relationship between ΔT_j and N_f :

$$\Delta T_j = \frac{A.N_f^{-a} + B.N_f^{-b}}{\alpha\, t_{on}^{\beta}} \tag{9}$$

The relation (9) gives the lifetime model (N_f) with a dependence on the stresses, i.e. junction temperature variations (ΔT_j) and heating duration (t_{on}). From, this relation it can be seen that if only low cycle fatigue domain is considered (high ΔT_j), only the Coffin-Manson law will be taken into account leading to typical empirical lifetime models as in [6,7].

For validation purpose, the model thus obtained has been tested on some additional experimental points from [3] where the same power modules were tested in power cycling conditions with different t_{on} values. The results used here are related to the wire bond failure only.

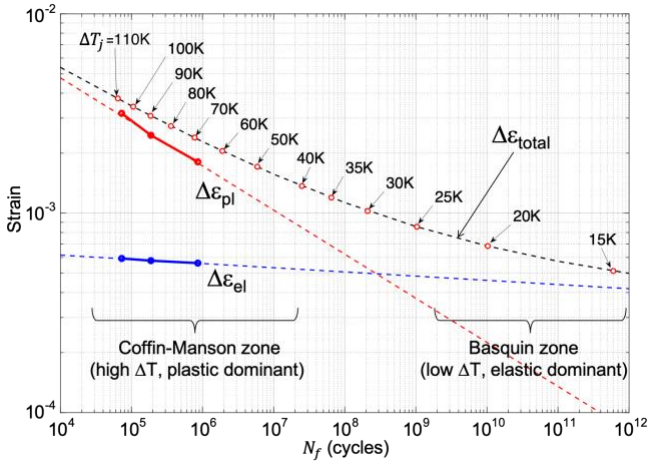

Fig.14: Total strain with lifetime and ΔT_j dependence

As results, all experimental N_f values are given in fig.15 with the dependence in ΔT_j. Experimental results from this paper (black circles and black disks) added to those from [3] (colored triangles) are visible in this figure. All the dotted curves in this figure are obtained by the model for the different indicated t_{on} values. It can be seen that the model (eq.9) is a fairly satisfactory representation of the experimental results as well as the test points used for the validation.

As already said above, the finite element model does not take into account the stress duration, the behavior laws used for aluminum being time-independent. So, even if this model was constructed on the basis of experimental results (N_f) and calculated strains for t_{on} = 3s, relation (6) combined with (7) makes it possible to obtain a model which, even referenced to t_{on} = 3s, gives valid results for a large scale of t_{on} values.

Finally, additional tests under low ΔT_j conditions must still be performed to validate the model in normal operative stress conditions.

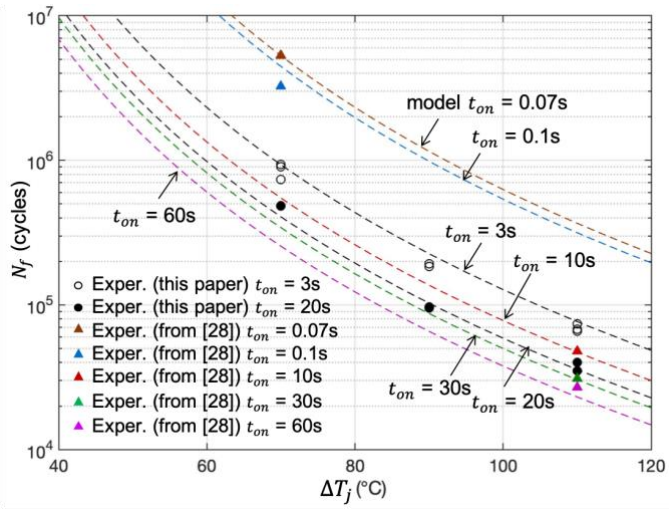

Fig.15: Power cycling test results and lifetime model validation

V. Conclusion

A stress-based lifetime model for bond wire contacts of Insulated Gate Bipolar Transistors (IGBT) power modules has been presented in this paper. The model is based on the

combination of two relationships. The first one is a relation between thermal stresses (ΔT_j, t_{on}) and strain, the second one is a relation between strain and lifetime. The first relation, issued from a numerical design of experiment, leads to a linear dependency of the strain with the thermal stress (ΔT_j) and a power law dependency with the stress duration (t_{on}). The second one is obtained from both the combination of experimental lifetime results from accelerated power cycling tests and strains from numerical results in same conditions than in testing. This last relation takes into account both Coffin-Manson's law and Basquin's law leading to a capability for the model to predict lifetime in high cycle conditions, i.e. low thermal stresses. The model has been tested and satisfactorily validated using additional power cycling test conditions from literature. Additional tests under low ΔT_j conditions must still be performed to validate the model in normal stress conditions.

REFERENCES

[1] V. Smet, F. Forest, J.J Huselstein, F. Richardeau, Z. Khatir, S. Lefebvre, M. Berkani, “Ageing and Failure Modes of IGBT Modules in High-Temperature Power Cycling”, IEEE Trans. on Industrial Electronics, vol. 58, n°10, pp. 4931-4941, 2011.

[2] J. Lutz, "Packaging and Reliability of Power Modules", 8th International Conference on Integrated Power Electronics Systems, CIPS 2014.

[3] M. Junghaenel, U. Scheuermann, "Impact of load pulse duration on power cycling lifetime of chip interconnection solder joints", Microelectronics Reliability, vol.76–77, pp.480–484, 2017.

[4] A. Morozumi, K. Yamada, T. Miyasaka, S. Sumi, Y. Seki, "Reliability of Power Cycling for IGBT Power Semiconductor Modules", IEEE Trans. on industry applications, Vol. 39, No. 3, 2003.

[5] I.F. Kovacevic-Badstuebner, J.W. Kolar, U. Schilling, "Modelling for the Lifetime Prediction of Power Semiconductor Modules", in "Reliability of power electronic converter systems", Chapt.5, pp.103-137, IET ed., 2015.

[6] M. Held, P. Jacob, G. Nicoletti, P. Scacco, andM.-H. Poech, “Fast power cycling test of IGBT modules in traction application,” Int. Journal of Electronics, vol.86, no.10, pp.1193–1204, 1999

[7] R. Bayerer, T. Herrmann, T. Licht, J. Lutz, and M. Feller, “Model for power cycling lifetime of IGBT modules - various factors influencing lifetime,” in Proc of 5th Int. Conf. on Integrated Power Systems (CIPS), pp.37–42, 2008.

[8] U. Scheuermann and R. Schmidt, “A new lifetime model for advanced power modules with sintered chips and optimized Al wire bonds,” in Proc. of Int. Conf. for Power Electronics, Intelligent Motion, Renewable Energy and Energy Management (PCIM), 2013, pp. 810–817.

[9] U. Drofenik, I. Kovacevic, R. Schmidt, and J.W. Kolar, “Multi-domain simulation of transient junction temperatures and resulting stress-strain behavior of power switches for long term mission profiles,” in Proc. of the IEEE Workshop on Control and Modeling for Power Electronics (COMPEL), pp. 1–7, 2008.

[10] P. Steinhorst, T. Poller, and J. Lutz, “Approach of a physically based lifetime model for solder layers in power modules,” Microelectronics Reliability, vol. 53, no. 8-10, pp. 1199–1202, 2013.

[11] O. Schilling, M. Schaefer, K. Mainka, M. Thoben, and F. Sauerland, “Power cycling testing and FE modelling focussed on Al wire bond fatigue in high power IGBT modules,” Microelectronics Reliability, vol. 52, no.9-10, pp. 2347–2352, 2012.

[12] G. Riedel, R. Schmidt, C. Liu, H. Beyer, and I. Alapera, “Reliability of large area solder joints within IGBT modules: Numerical modeling and experimental results,” in Proc. of Int. Conf. on Integrated Power Systems (CIPS), pp.288–298, 2012.

[13] L. Yang, P. A. Agyakwa, and C. M. Johnson, “A time-domain physics-of-failure model for the lifetime prediction of wire bond interconnects,” Microelectronics Reliability, vol. 51, no. 9-11, pp. 1882–1886, 2011.

[14] L. Yang, P. A. Agyakwa, and C. M. Johnson, “Physics-of-failure lifetime prediction models for wire bond interconnects in power electronic modules,” IEEE Trans. Device Mater. Rel., vol. 13, no. 1, pp. 9–17, 2013.

[15] S. Deplanque, W. Nuchter, B. Wunderle, R. Schacht, B. Michel, “Lifetime prediction of SnPb and SnAgCu solder joints of chips on copper substrate based on crack propagation FE-analysis,” in Proc. of 7th Int. Conf. on Thermal, Mechanical and Multiphysics Simulation and Experiments in Micro-Electronics and Micro-Systems (EuroSime), 2006.

[16] T. Matsunaga, Y. Uegai, "Thermal Fatigue Life Evaluation of Aluminum Wire Bonds", Electronic System integration Technology Conference, Dresden, 2006.

[17] K. Sasaki, N. Iwasa, T. Kurosu, K. Saito, Y. Koike, Y. Kamita et al., “Thermal and structural simulation techniques for estimating fatigue life of an IGBT module” in Proc. 20th Int. Symp. Power Semicond. Devices IC’s, Orlando, USA, pp. 181–184, 2008.

[18] H. Huang and P.A. Mawby, “A lifetime estimation technique for voltage source inverters”, IEEE Trans. Power Electron., vol.28, no.8, pp.4113–4119, 2013.

[19] E. Zio, G. Peloni, "Particle filtering prognostic estimation of the remaining useful life of nonlinear components", Reliability Engineering and System Safety, vol.96, pp.403–409, 2011.

[20] J. Celaya, A. Saxena, S. Saha, K. Goebel, "Prognostics of Power MOSFETs under Thermal Stress Accelerated Aging using Data-Driven and Model-Based Methodologies", in Proc. of PHMC, 2011.

[21] B. Saha, J. R. Celaya, P. F. Wysocki, and K. F. Goebel, “Towards prognostics for electronics components,” in Proc. IEEE Aerospace Conf., pp.1–7, 2009.

[22] A. Alghassi, "Prognostics and Health Management of Power Electronics", PhD Thesis, Cranfield University, 2016

[23] D. Astigarraga et al., "D Analysis of the Results of Accelerated Aging Tests in Insulated Gate Bipolar Transistors", IEEE Trans. On Power Electronics, vol.31, N°11, pp.7953-7962, 2016.

[24] C. Chen et al., "PHM Application of Power Converters Using Health Precursor of Power MOSFETs", PHM Conference-Beijing, 2015.

[25] S.S. Manson, "Thermal Stress Low-cycle Fatigue", McGraw-Hill, 1966.

[26] B. Joadder, J. Shit, S. Acharyya, S. Dhar, "Fatigue Failure of Notched Specimen — A Strain-Life Approach", Materials Sciences and Applications, vol.2, pp.1730-1740, 2011.

[27] O. H. Basquin, “The Exponential Law of Endurance Tests,” American Society for Testing and Materials Proceedings, Vol.10, pp.625-630, 1910.